High-Throughput Study of Diffusion and Phase Transformation Kinetics of Magnesium-Based Systems for Automotive Cast Magnesium Alloys – Ohio State University

Project Details:

Alan A. Luo, Principle Investigator
The Ohio State University
137 Fontana Labs, 116 W. 19th Ave.
Columbus, OH 43210
Phone: 614-292-5629
E-mail: luo.445@osu.edu

Ji-Cheng Zhao, Principle Investigator
The Ohio State University
286 Watts Hall, 116 W. 19th Ave.
Columbus, OH 43210
Phone: 614-292-9462
E-mail: zhao.199@osu.edu

Adrienne Riggi, Project Officer
National Energy Technology Laboratory
3610 Collins Ferry Road P.O. Box 880
Morgantown, WV 26507-0880
Phone: 304-285-5223
E-mail: Adrienne.riggi@netl.doe.gov

William Joost, DOE Technology Development Manager
U.S. Department of Energy
1000 Independence Ave., S.W.
Washington, DC 20585
Phone: 202-287-6020
E-mail: william.joost@ee.doe.gov

Contractor: Ohio State University, CompuTherm LLC (Madison, WI)
Contract No.: DE-EE0006450

Abstract/Executive Summary

The objective of the proposed study is to establish a scientific foundation on kinetic modeling of diffusion, phase precipitation, and casting/solidification, in order to accelerate the design and optimization of cast magnesium (Mg) alloys for weight reduction of U.S. automotive fleet. The team has performed the following tasks: 1) study diffusion kinetics of various Mg-containing binary systems using high-throughput diffusion multiples to establish reliable diffusivity and mobility databases for the Mg-aluminum (Al)-zinc (Zn)-tin (Sn)-calcium (Ca)-strontium (Sr)-manganese (Mn) systems; 2) study the precipitation kinetics (nucleation, growth and coarsening) using both innovative dual-anneal diffusion multiples and cast model alloys to provide large amounts of kinetic data (including interfacial energy) and microstructure atlases to enable implementation of the Kampmann-Wagner numerical model to simulate phase transformation kinetics of non-spherical/non-cuboidal precipitates in Mg alloys; 3) implement a micromodel to take into account back diffusion in the solid

phase in order to predict microstructure and microsegregation in multicomponent Mg alloys during dendritic solidification especially under high pressure die-casting (HPDC) conditions; and, 4) widely disseminate the data, knowledge and information using the Materials Genome Initiative infrastructure (http://www.mgidata.org) as well as publications and digital data sharing to enable researchers to identify new pathways/routes to better cast Mg alloys.

Accomplishments

- **High throughout experiments:** Diffusion multiple and liquid-solid diffusion couples including Mg-Al, Zn, Sn, Y, Ca, Nd, Sr, Ce, Gd, Mn and Li systems were prepared and subjected to heat treatment at various temperatures to study the diffusion and generate a series of composition profiles.

- **The first comprehensive mobility database for Mg alloys:** Forward-simulation analysis was employed to extract both the impurity and interdiffusion coefficients from diffusion profiles measured by electro probe microanalysis (EPMA). Diffusion data for Mg-Al, Zn, Sn, Y and Ca systems were critically evaluated with all other available literature data. The best-judgment diffusion coefficients as a function of temperature are determined. All the diffusion data are used as input to establish the first comprehensive mobility database for Mg alloys.

- **CALPHAD-based micromodel for solidification:** PanSolidification, coupled with PanMg thermodynamic database and the Mg mobility database newly developed in this project, were successfully applied to simulate the evolution of solidification microstructure of both binary and ternary Mg alloys under directional solidification and die casting conditions. In simulating microsegregation behavior, the solidification micromodel takes into accounts of both back diffusion and geometry of solidification dendritic structures. The simulation results are in good agreement with experimental results.

- **KWN-based precipitation model:** PanPrecipitation, coupled with PanMg thermodynamic database and the new mobility database, was successfully used to simulate the evolution of precipitation microstructure in Mg-Al-Sn based Mg alloys. The simulation results on binary Mg-Sn and Mg-Al were comparable to experimental results. The simulation of precipitation kinetics in ternary Mg-Al-Sn system shows that the precipitation kinetics of Mg_2Sn phase in ternary system is much faster than that in binary Mg-Sn systems, indicating alloying may be an effective method to speed up the precipitation kinetics in Mg-Sn systems.

- **Mg-Al-Sn alloy optimization:** Using the above developed ICME models, the effects of alloying additions on the precipitation kinetics in Mg-Al-Sn system were investigated. It was discovered that mall additions of Ag and Zn can significantly accelerate the precipitation kinetics in Mg-Sn system, while other alloying elements such as Ca and Cu have detrimental effects.

Introduction

The lack of diffusivity data for Mg alloys is hindering the computational design of high performance Mg alloys using Integrated Computational Materials Engineering (ICME) approach. Compared with Al alloys, information on solidification and precipitation kinetics (nucleation, growth and coarsening) of Mg alloys is not sufficient and needs to be investigated by a combination of experiment and simulation. A micromodel considering back diffusion and cooling rate is important for accurately simulating the solidification of Mg alloys, especially prepared in actual casting conditions. Solid-liquid diffusion couples for Mg-MgY, MgGd, MgCe, MgMn, Li systems were prepared and heat treatments were conducted at various temperatures to generate diffusion profiles for EPMA measurements. The diffusivities for Al, Zn, Sn, Ca, Y were extracted

from diffusion profiles by the forward simulation method [1]. With CALPHAD approach [2], the first version of CALPHAD-type Mg atomic mobility database within this project was completed and used in the design of solution treatment schedule, precipitation and solidification simulations. The simulations of microstructure evolution of AZ91 (Mg-9wt%Al-1wt.%Zn) and Mg-Sn alloys during aging were updated with the new database. AT72 (Mg-7wt%Al-2wt.%Sn) alloy was microalloyed with Zn, Ag, Ca, Cu and the aging hardening responses were measured. The microsegregation data for Mg-Al, Mg-Al-Ca and Mg-Al-Ca-Sn alloys from literature and this project were compiled. The PanSolidification module was used to simulate the non-equilibrium solidifications of several binary Mg-Al and ternary Mg-Al-Ca alloys prepared by directional solidification. HPDC AT72 alloy was prepared to provide microsegregation data for further development of the PanSolidification module.

Main results

1. Diffusion

Two types of diffusion samples are employed to study the diffusion in Mg-based systems. The first type is the diffusion multiple which is a high throughput technique to study solid diffusion. Another novel liquid-solid diffusion couple developed in this project is used to study the diffusion at elevated temperatures above eutectics of Mg binary systems. The schematic of the diffusion multiples and liquid-solid diffusion couples are shown in Figure 1. EPMA was used to measure the diffusion profiles from annealed and quenched diffusion samples. The forward-simulation analysis [1] was employed to extract both the impurity and interdiffusion coefficients. With the two diffusion experiment methods, the diffusion of Mg-Al, Zn, Sn, Y, Ca, Nd, Sr, Ce, Gd, Mn and Li systems at a wide temperature range has been studied in this project.

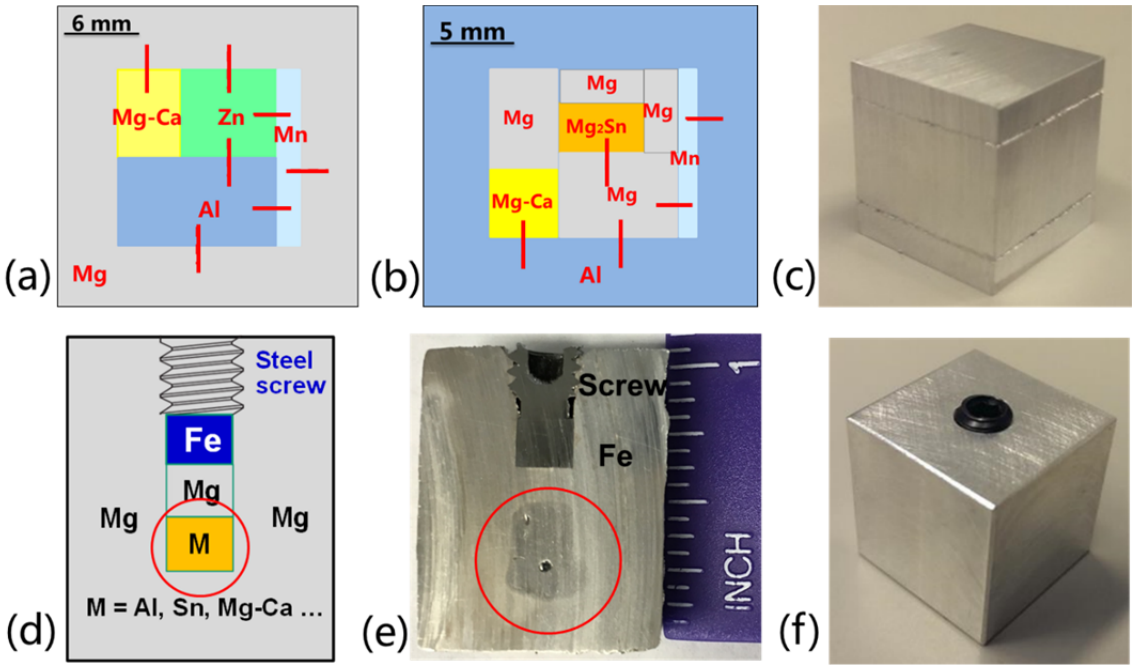

Figure 1. (a) and (b) design of diffusion multiples; (c) photo of a welding-sealed diffusion multiple; (d) design of a liquid-solid diffusion couple; (e) a cross section of a liquid-solid diffusion couple after annealing and quenching; and (f) a photo of a assembly of liquid-solid diffusion couple.

The combined diffusion multiples/liquid-solid diffusion couples and the forward simulation method were employed to reliably extract diffusion coefficients of Al, Zn, Sn, Y and Ca in Mg. The diffusion data were critically evaluated with available literature data. The best-judgment impurity diffusion coefficients of the five solutes are determined, which serve as the foundation of the Mg diffusivity database. The maximum solubility values of these five solutes in HCP Mg phase are also determined, as shown in Table. 1. The diffusion profiles of Mg-Li, Gd, Ce and Mn systems are also obtained.

The diffusion data of Mg-Al, Zn, Sn, Y and Ca systems are summarized in Figures 3-7. The consentaneous experimental impurity diffusion coefficients expressed by Arrhenius equations for these systems are shown as solid red lines in the plots and the expressions are summarized in Table 1. The optimized equation for the Mg-Al system is based on our data and other two diffusion couple studies by Kammerer et al. [5] and Brennan et al. [6] excluding Das et al. [7] and the study using the secondary ion mass spectrometry (SIMS) by Brennan et al. [8]. As for the Mg-Zn system, the final equation is based on our data and the data from diffusion couple from Kammerer et al. [5], tracer data from Lal [9] and Čermák and Stloukal [10] excluding data from Das et al. [11]. The equation for the Mg-Sn system is recommended by fitting our data and tracer data from Combronde and Brebec [12].

Since pure Y is very prone to oxidation, a Mg-25wt.%Y master alloy was used to assemble three Mg-Y liquid-solid diffusion couples, which were annealed at elevated temperatures. The interdiffusion coefficients are constant at each temperature and thus equal to the impurity diffusion coefficients of Y in Mg. The diffusion data reported by Das et al. [13] obtained from a multiphase simulation analysis are again significantly lower than our values in trend, similar to the situations for Mg-Al, Zn systems. We performed the forward simulations on four original Mg-Y diffusion profiles provided by Das et al. [13] and obtained impurity and interdiffusion coefficients that agree well with our diffusion coefficients, indicating that their experimental profiles for Mg-Y are reliable, but the analysis process may be problematic. The final Arrhenius equation is determined using our data and re-analyzed data from Das et al. [13].

A Mg-15 wt.% Ca master alloy was used to assemble four Mg-Ca liquid-solid diffusion couples due to high reactivity of pure Ca. It is worthwhile noting that the solubility of Ca in Mg is extremely limited (as low as 0.08 at.% at 630 °C), but very accurately determined by EPMA composition profiling from these liquid-solid diffusion couples. At such low solubility values, it is reasonable to assume that the interdiffusion coefficients are constant at each temperature and are equal to the impurity diffusion coefficients of Ca in Mg. Our data is the first set of experimental impurity diffusion coefficients reported.

Tracer experiments, though laborious and expensive to perform, are usually very reliable in determining the impurity diffusion coefficients. Three sets of tracer experiments were performed for Sn and Zn diffusion in Mg [9, 10, 12], and there is an excellent agreement between our data and the results of these tracer studies, demonstrating the reliability of our combined approach in obtaining accurate impurity diffusion coefficients. There are three first-principles studies on impurity (dilute) diffusion coefficients in Mg [14–16] and the calculation results have been compared for each system in Figures. 3b, 4b, and 5-7. The calculations of Zhou et al. [14] are a recent improvement over those of Ganeshan et al. [15], thus the results of Ganeshan et al. [15] are not used in the following comparison. Figure 8 is a comprehensive comparison for all five elements, showing that recent calculations from Zhou et al. [14] and Wu et al. [16] have achieved an impressive accuracy for Al, Sn and Zn. However, the calculated impurity coefficients of Ca in Mg from both groups are higher than our experimental values and the computed impurity coefficients of Y in Mg from Wu et al. [16] are also higher than our experimental values. The results for Y from Zhou et al. [14] agree well with our experimental data. The calculated diffusion coefficients along the basal plane and along the c-axis are averaged (2/3 basal + 1/3 c-axis) into a single impurity diffusion coefficient for this comparison according to literature [17]. Such an element-by-element comparison using reliable experimental data is very valuable in identifying ways to improve the reliability of future calculations.

Finally, Figure 9 summarizes the best-judgment/consentaneous experimental impurity diffusion coefficients of Al, Ca, Sn, Y and Zn in Mg in comparison with the self-diffusion coefficient of Mg [18] (We averaged

diffusion coefficients along the basal plane and the c-axis into one Arrhenius equation $D_{Mg\ in\ Mg} = 1.66 \times 10^{-4} e^{-138440/RT}$ (m^2/s)). These impurity diffusion coefficients should be very reliable and applicable to a wide range of temperatures. These data together with the interdiffusion coefficients obtained in this project as well as literature data will serve as the foundation for reliable diffusion (mobility) databases for Mg alloys. Among the five elements, Ca has the highest and Zn has the second highest impurity diffusion coefficient in Mg, both higher than the Mg self-diffusion coefficient. In the absence of experimental diffusion data, Ca has been often assumed to be a slow diffuser in Mg as rare earth elements. Our results, however, clearly show that Ca diffusion in Mg is significantly faster than the Mg self-diffusion which is faster than the Al diffusion in Mg. The fast Ca diffusion may be a disappointment to researchers who assumed slow Ca diffusion in Mg may help achieve high creep strength in Ca-alloyed Mg alloys for high temperature applications. Both Al and Sn have very similar impurity diffusion coefficients in Mg and they diffuse slower than the Mg self-diffusion. Y diffusion in Mg is slightly slower than Al and Sn at high temperatures, but about the same as Sn below 390 °C, thus Y may not be as a potent element for enhancement of creep strength of Mg alloys as has been often expected.

Diffusion samples of Mg-Nd, Sr, Gd, Li, Ce and Mn systems were also prepared. There were some difficulties in studying the diffusion of these systems. Sr is a very reactive element and has very low solubility in Mg. Although Mg-Sr liquid-solid diffusion couples were successfully annealed in our work, the diffusion profiles cannot be reliably determined due to the measurement limit of EPMA. Li is also a very active element and liquefies easily. The Mg-Li liquid-solid diffusion couples were thus assembled in glove box with high purity Ar atmosphere. The atom of Li is so light that the composition of Li in the obtained diffusion samples cannot be measured by EPMA. Therefore, the diffusion profiles of Mg-Li are determined by measuring the Mg composition in the couple. Mn and other rare earth elements have relatively high melting points compared to Mg as well as other solutes in Mg. Therefore, the Mg binary alloys with these elements were used to assemble the liquid-solid diffusion couples. Some diffusion profiles obtained are shown in Figure 10. The diffusion coefficients will be extracted using forward-simulation analysis afterwards.

Table I: Maximum solubility of Al, Zn, Sn, Y and Ca in Mg and recommended impurity diffusion coefficients as Arrhenius equations (in m^2/s with temperature T in Kelvin and the gas constant R = 8.314 J K^{-1} mol^{-1}).

System	Solubility (at.%) of solute at annealing Temperature (°C)	Impurity diffusion coefficient as Arrhenius equation
Mg-Al	10.3, 7.2, 4.6, 2.5 at.% Al at 450, 500, 550, 600 °C	$D_{Al\ in\ Mg} = 2.0 \times 10^{-4} e^{-146000/RT}$
Mg-Zn	3.5, 2.6, 1.7 at.% Zn at 450, 500, 550 °C	$D_{Zn\ in\ Mg} = 0.87 \times 10^{-4} e^{-125000/RT}$
Mg-Sn	0.8, 1.1, 2.0, 4.1, 2.6 at.% Sn at 375, 420, 500, 550, 600 °C	$D_{Sn\ in\ Mg} = 1.08 \times 10^{-4} e^{-140900/RT}$
Mg-Y	1.9, 1.0, 0.6 at.% Y at 590, 610, 630 °C	$D_{Y\ in\ Mg} = 0.08 \times 10^{-4} e^{-126700/RT}$
Mg-Ca	0.44, 0.26, 0.22, 0.08 at.% Ca at 530, 580, 600, 630 °C	$D_{Ca\ in\ Mg} = 0.06 \times 10^{-4} e^{-103700/RT}$

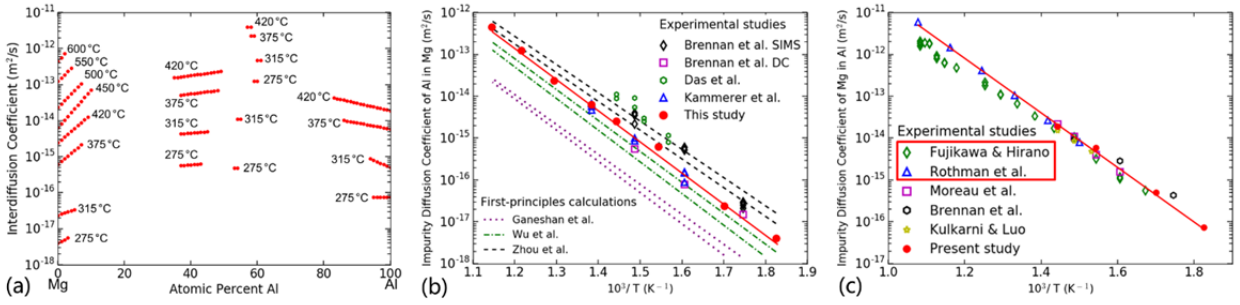

Figure 3. Results for the Mg-Al system: (a) Interdiffusion coefficients of Mg-Al; (b) Al impurity diffusivity in Mg; and (c) Mg impurity diffusivity in Al.

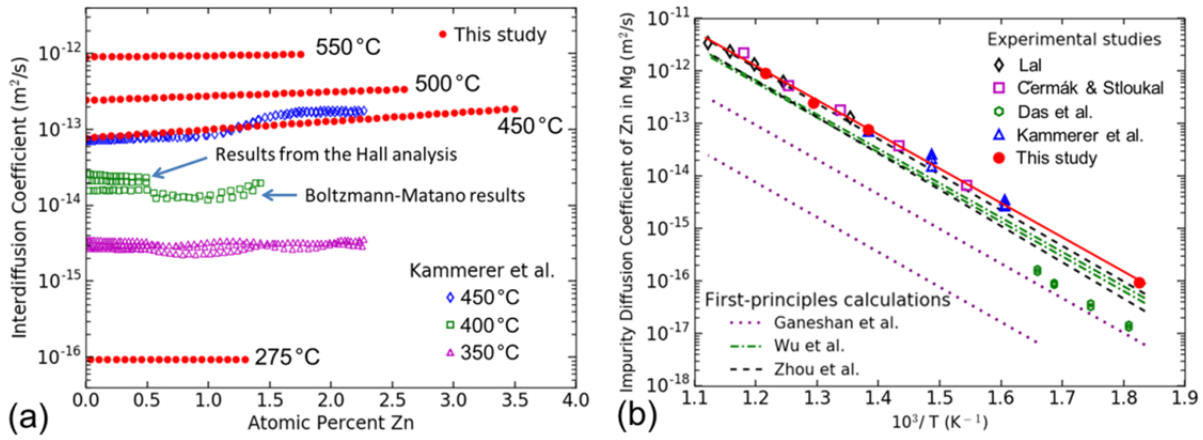

Figure 4. Results for the Mg-Zn system: (a) Interdiffusion coefficients for the hcp phase of the Mg-Zn system; and (b) Zn impurity diffusivity in Mg.

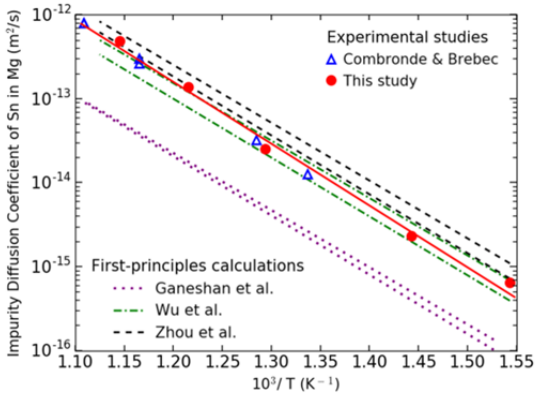

Figure 5. Comparison of experimental impurity diffusion coefficients of Sn in Mg with first-principles calculations.

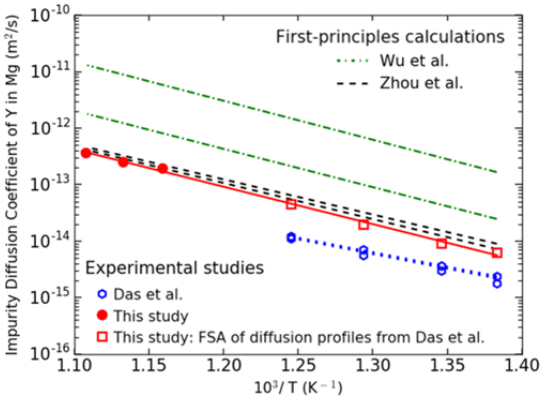

Figure 6. Comparison of experimental impurity diffusion coefficients of Y in Mg with first-principles calculations.

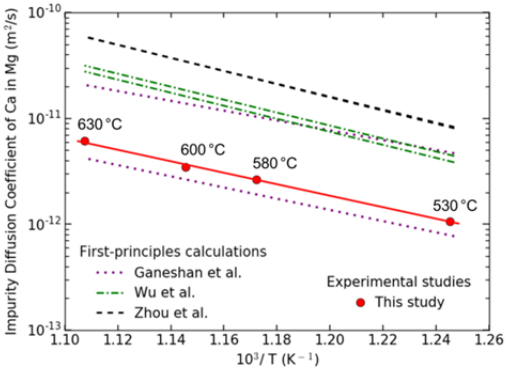

Figure 7. Comparison of experimental impurity diffusion coefficients of Ca in Mg with first-principles calculations.

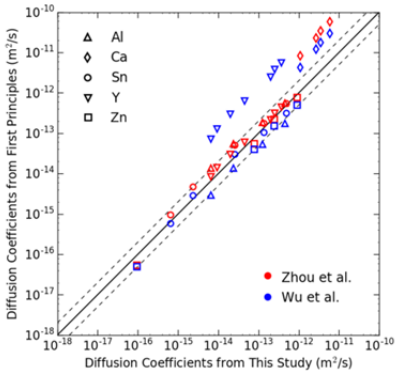

Figure 8. Comparison of the experimental impurity diffusion coefficients with first-principles calculations (The dashed lines refer to values that are either twice as much or half the values).

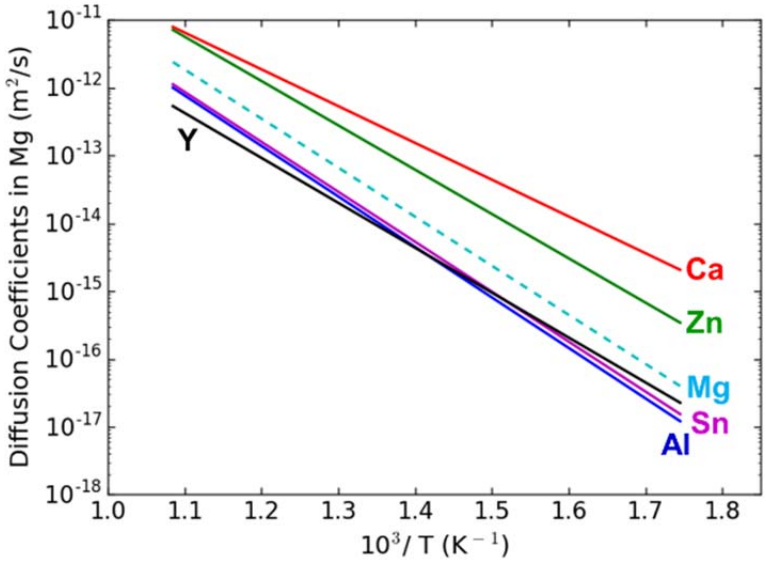

Figure 9. Comparison of the best-judgement impurity diffusion coefficients of Al, Zn, Sn, Y and Ca in Mg with the self-diffusion coefficient of Mg.

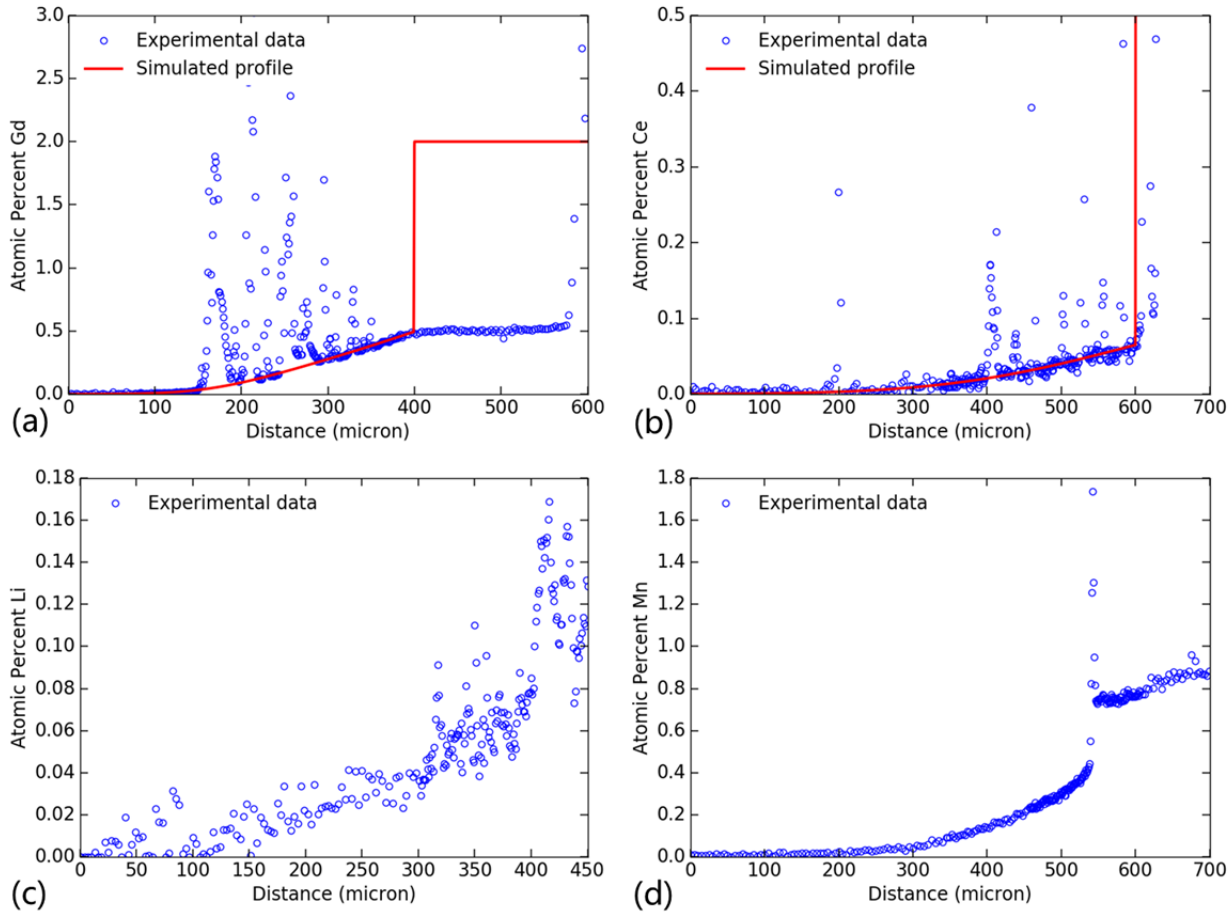

Figure 10. Diffusion profiles: (a) Mg-Gd; (b) Mg-Ce; and (c) Mg-Li and (d) Mg-Mn systems.

2. Solidification

PanSolidification module was directly coupled with PanMg thermodyanmic database and mobility database considering thermodynamic and diffusion effects including undercooling, solid state back-diffusion, dendrite arm coarsening and thermodynamic correction of the interface concentrations. Figure 11 shows the flow chart of the PanSolidification module used in this project. The input variables for simulation consists of alloy composition (x), solidification velocity (V), thermal gradient (G), solid/liquid interfacial energy (γ), latent heat (H) etc. Cooling rate (CR) is automatically calculated as $CR=G\times V$. In this project, the PanSolidification module was sucessfully used to simulate the solidification of directionally solidified (DS) Mg-Al alloys under different cooling rates, and extended to simulations on ternary directionally solidified Mg-Al-Ca alloys and die casting Mg-Al-Sn system. For DS specimens, the cooling rates can be well controlled. Those specimens can help calibrate PanSolidification module. Die casting is one of the most efficient and economic methods for producing magnesium components in industrial scales. The cooling rates involved in die casting are much higher as compared with those in directional solidification. In this project, AT72 magensium alloy specimens were prepared in die casting. The microsegregation behavior in those alloys were also investigated using PanSolidification module.

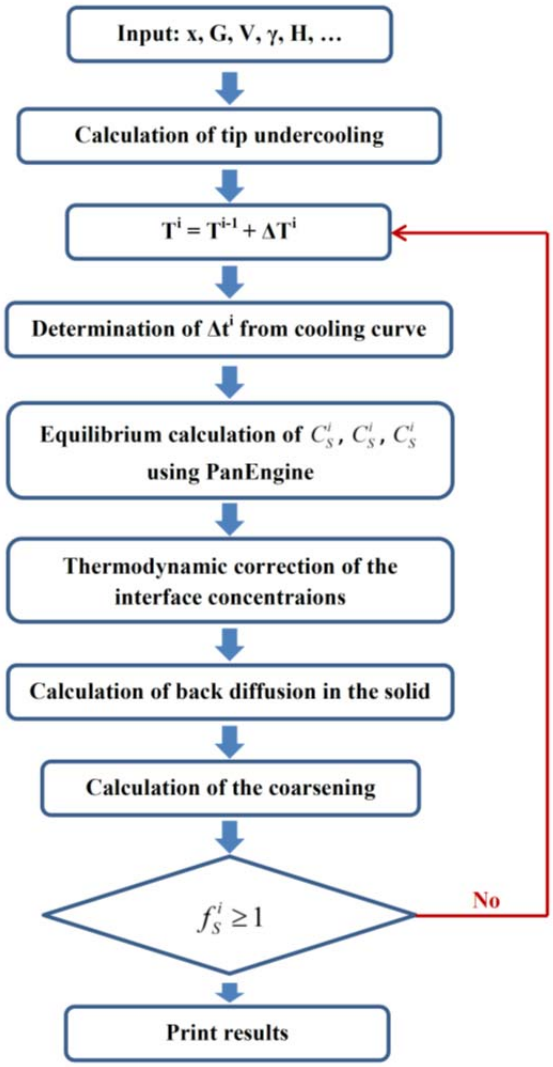

Figure 11. Flow chart of the PanSolidification module.

The microsegregation behavior of magnesium alloys can be quantitatively characterized using Electron Microprobe Analyzer (EPMA). To achieve statistical results of microsegregation of different alloying elements, test grids consisting of 400 data points with an inter-space ranging from 10 µm to 20µm were uniformly placed on a sample area covering several grains. At each grid point, the chemical compositions of alloying elements were measured using EPMA. Figure 12a) show an example of such testing grid overlapped on a BSE-SEM image of the microstructure of a directional solidification Mg-8.12Al-1.55Ca-2.91Sn alloy. The collected compositions of different alloying elements can be further sorted using Flemings-Gungor method [19]. Figure 12 b) shows an example of sorted composition profile of Al in the directional solidification Mg-8.12Al-1.55Ca-2.91Sn alloy.

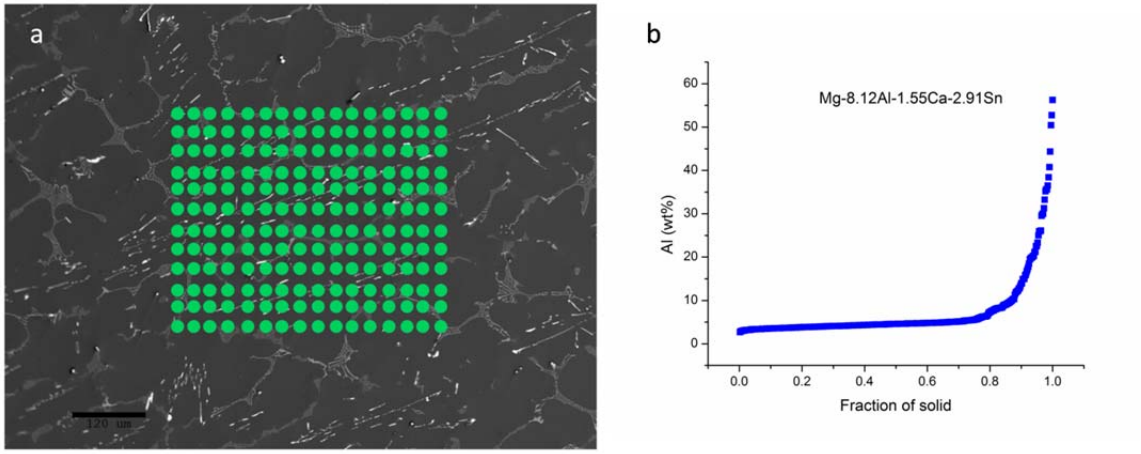

Figure 12. Quantitative characterization of microsegregation of alloying elements in magnesium alloys: a) an example of EPMA testing grid overlapped on a BSE-SEM image; and b) an example of a sorted composition profile of Al based on quantitative EPMA analysis.

The microsegregation data for binary Mg-Al and ternary Mg-Al-Ca alloys prepared by directional solidification from literature [20-23] and current experiments were collected and compiled. Table 2 lists the experimentally investigated Mg-Al and Mg-Al-Ca alloys in literature [20-23] under various cooling rates. Solidification simulations are carried out on these binary and ternary alloys using the PanSolidification module.

Table 2: Binary and ternary magnesium alloys used for solidification simulation

Alloy composition (wt.%)	Thermal gradient (K/m)	Solidification velocity (m/s)
Mg-3Al	$7.5x10^{3}$	$5.0x10^{-5}$
Mg-3Al	$4.26x10^{2}$	$2.58x10^{-3}$
Mg-4Al	$4x10^{3}$	$5.0x10^{-5}$
Mg-4Al	$4x10^{3}$	$2.0x10^{-4}$
Mg-6Al	$7.5x10^{3}$	$5.0x10^{-5}$
Mg-6Al	$4.26x10^{2}$	$2.58x10^{-3}$
Mg-9Al	$7.5x10^{3}$	$5.0x10^{-5}$
Mg-9Al	$4.26x10^{2}$	$2.58x10^{-3}$
Mg-4Al-4Ca	$4x10^{3}$	$5.0x10^{-5}$
Mg-4Al-4Ca	$4x10^{3}$	$1.0x10^{-4}$
Mg-5Al-3Ca	$4x10^{3}$	$1.0x10^{-6}$
Mg-5Al-3Ca	$4x10^{3}$	$3.0x10^{-5}$
Mg-5Al-3Ca	$4x10^{3}$	$1.0x10^{-4}$

Figures 13 and 14 show the calculated concentration profiles using different models (Scheil, Plate, Cylinder, and Sphere) for two binary Mg-Al alloys listed in Table 2. The experimental data obtained [22] under different cooling rates are also plotted on these figures for comparison. Three dendrite arm geometries, i.e. plate, cylinder and sphere, were considered in the present study. The morphology and scale of the dendrite structure are of crucial importance since they strongly influence the extent of back diffusion.

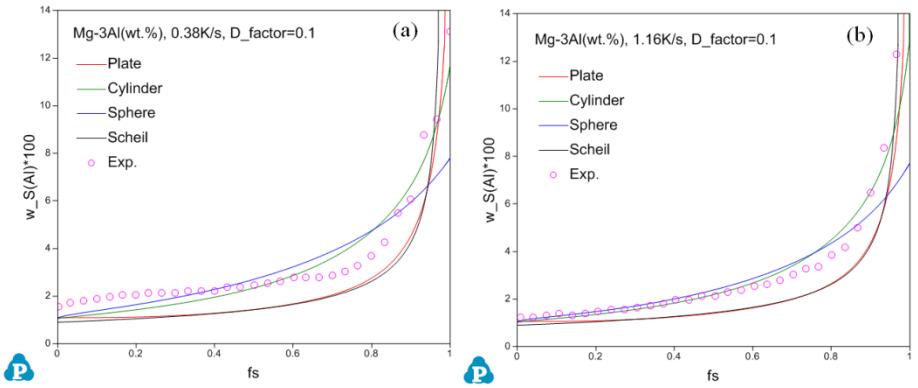

Figure 13. Simulated concentration profiles of Mg-3wt.%Al using different models with experimental data under different cooling rates: (a) 0.38K/s; and (b) 1.16K/s.

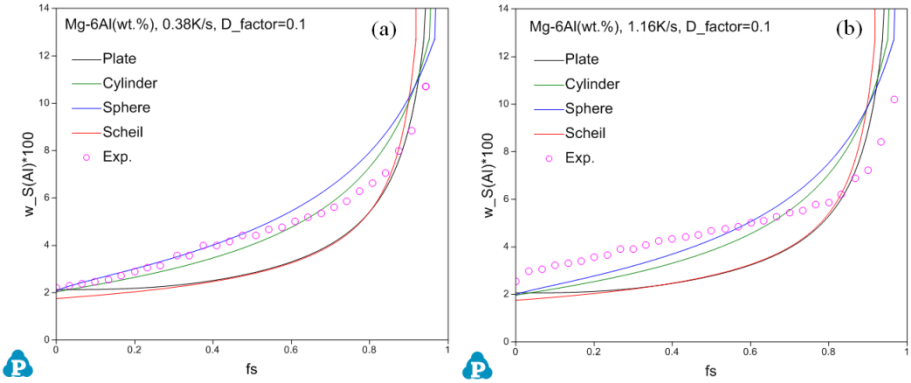

Figure 14. Simulated concentration profiles of Mg-6wt.%Al using different models with experimental data under different cooling rates: (a) 0.38K/s; and (b) 1.16K/s.

The results indicate that the calculated concentration profiles using the Scheil model are in large discrepancies with the experimental measurements. When back-diffusion effect is considered, the calculations show better agreement. In most cases, the sphere model yields the best agreement with the experimental data especially at lower fractions of solid. On the other hand, the calculated data using the plate geometry are in better agreement with the experimental at higher fractions of solids. The trend of the cylinder model is in between the sphere and plate models. It is well know that the formation and growth of the secondary arms at the earlier stage is in particle shape, the dendrite arm lengths are limited and the end effects play an important role. Therefore, the sphere arm morphology is the best to approximate the shape of the dendrite arms at this stage. As the dendrite arm grows continually, the end effects become less important and the plate model is a better approximation. This is the reason none of these model can describe the experimental data perfectly during the whole process. However, the development of a new morphology model for better describing the dendritic morphology at different solidification stages are far more complex and beyond the scope this project.

In addition to the concentration profiles, the simulated SDAS vs. the measured values are shown in Figure 15. One can see that the calculated SDAS values are slightly greater than the experimental measurements. This is because that we use the constant interfacial energy for simplicity and extendibility of the current PanSolidification module. As discussed in the Ref. [24], the interfacial energy decreases with the increasing Al concentration. The values we used is the same as derived for 3wt.% Al which is greater than that of higher Al concentrations (4, 6, and 9wt.%Al). Therefore the calculated SDAS results are slightly greater than the measured values. Comparison between the calculated and measured fractions of interdendritic phases is shown in Figure 16. It indicates that the plate model works better for the lower Al concentration and sphere model is better for the higher Al concentration.

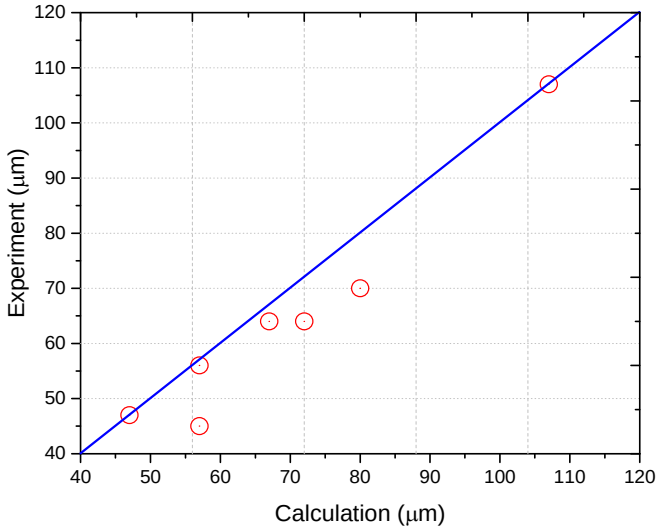

Figure 15. Comparison between the measured and simulated SDAS of Mg-Al binary alloys.

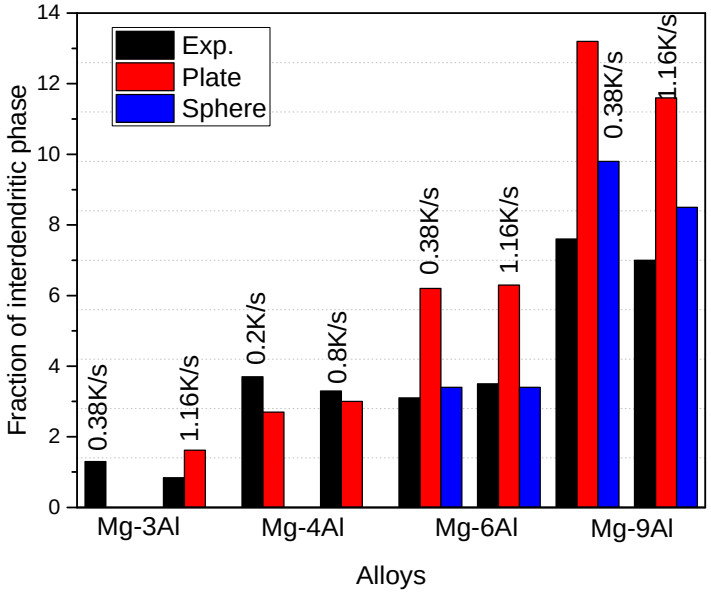

Figure 16.Comparison between the measured and simulated fraction of interdendritic phase region.

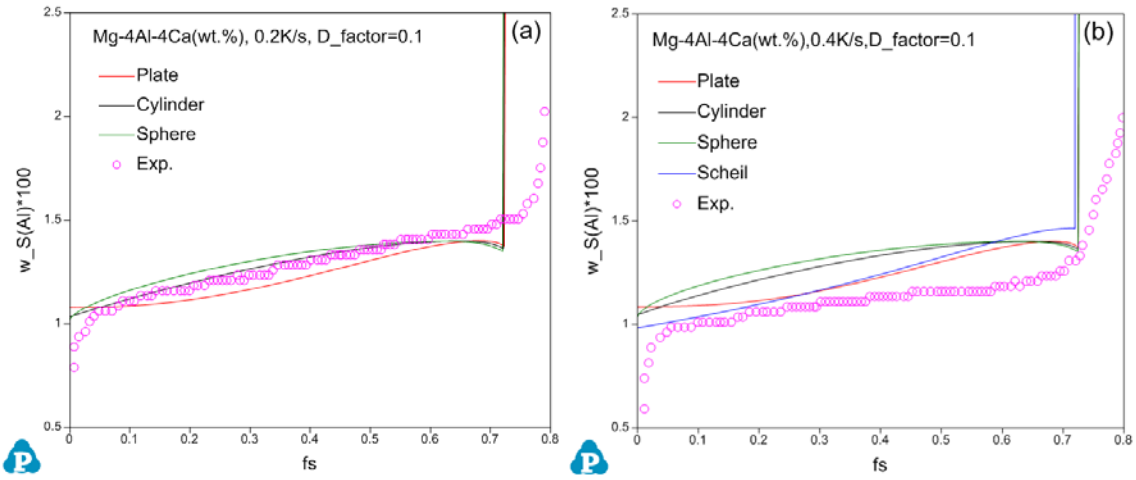

Figure 17. Simulated concentration profiles of Mg-4Al-4Ca (wt.%) using different models with experimental data under different cooling rates: (a) 0.2K/s; and (b) 0.4K/s.

Without adjusting any solidification parameters, the concentration profiles of the Mg-Al-Ca ternary alloys are simulated using various models as shown in Figure 17. The experimentally measured data are superimposed in the same figures as well. As shown in Figure 7a, the simulated concentration profiles are in good agreement with the experimental data for the Mg-4Al-4Ca alloy at the cooling rate of 0.2K/s, while large discrepancy is found between the simulated data and experimental values at the cooling rate of 0.4K/s as shown in Figure 7b. Here we want to point out that the experimentally measured concentration profile of Mg-4Al-4Ca at 0.4K/s is even lower than the Scheil simulations, which indicates that the experimental data may not be accurate. Comparison between the simulated and measured SDAS for the Mg-Al-Ca alloys is shown in Figure 18, which indicates that the simulated values are in good agreement with experimentally measured data.

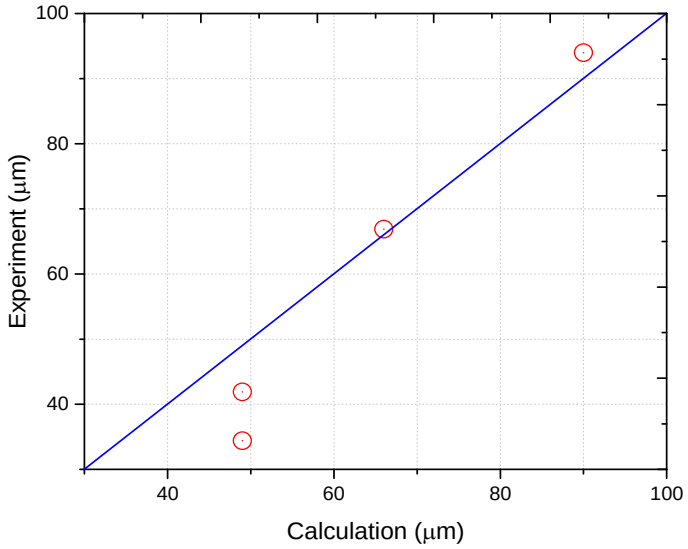

Figure 18. Comparison between the measured and simulated SDAS of Mg-Al-Ca ternary alloys.

The PanSolidification module was further applied to simulate microsegregation behavior associated with die casting process. AT72 magnesium testing samples were prepared using die casting. The cooling curve associated with the solidification of the samples were experimentally measured at the center of casting ingot and also simulated using ProCast™ software. Figure 19 shows both the experimental measurement and simulation results of the cooling curves. It can be seen that ProCast simulation can successfully capture main features of the experimental cooling curve. However, the simulation curve shifts to the right in Figure 19 with respect to the experimental cooling curves. This is possibly due to the fact that in simulation, it need about 0.5 second to allow the molten alloy to fill the center location of casting mold. The mesured cooling curve may provide accurate inputs for PanSolidification modeling.

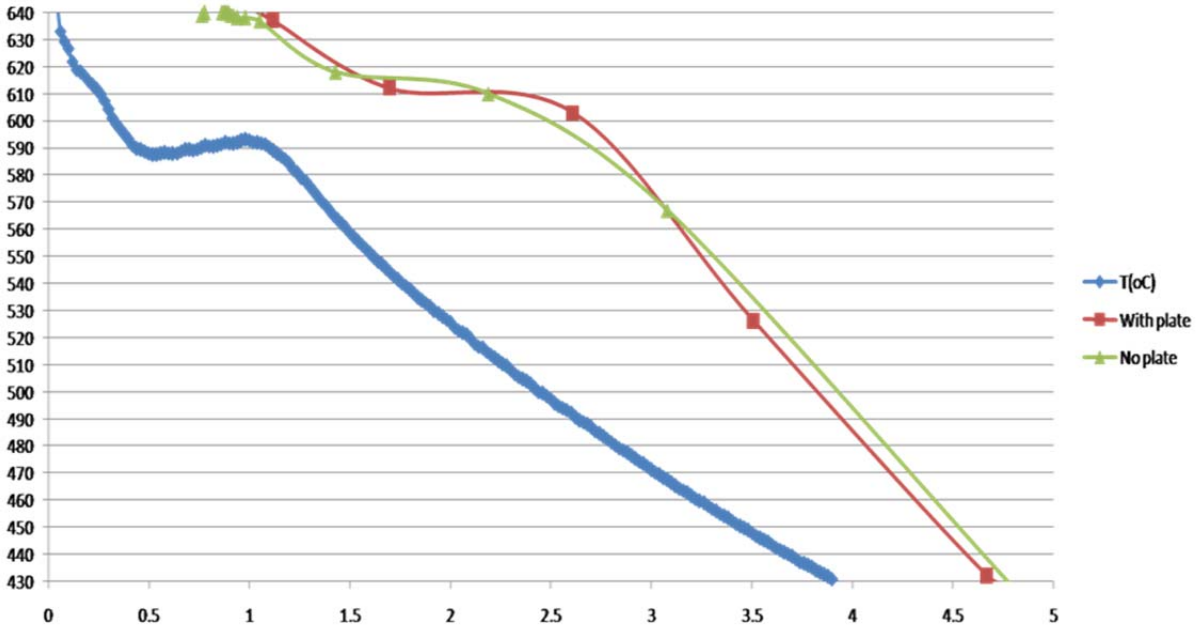

Figure 19. Experimental measurement of cooling curve and Procast simulation with or without consideration of the effect of cooling plate beneath the casting mold.

Figure 20a) shows the as-cast microstructure of AT72 magnesium alloy. Due to the fast cooling rates associated with solidification process, its microstructure has fine primary α cell in the order of a few microns. Figure 20b) shows the calculated concentration profiles of Al and Sn for AT72 alloy. The solid lines are calculated using the Scheil model for both Al and Sn. The results calculated using the Lever-rule model are shown in dashed lines. The symbols are EPMA measurements in this study. As mentioned above, the AT72 sample was prepared using die-casting. The solidification process is under high cooling rates. On the basis of experience, this experimental data should be much closer to the results of Scheil than Lever-rule. However, large discrepancies are found between the experimental data and calculated results. There are several possibilities from either experimental measurement and/or calculation. Here, we would like to mention that the EPMA measurement for the die casting sample is extremely difficult due to the relatively small sizes of primary Mg cells. There is an interaction volume when electron beam interacts with specimens. The size of interaction volume depends on accelerating voltage: the higher accelerating voltage, the larger interaction volume which usually ranges from 1 to 10 micron in diameter. For die casting microstructure with fine primary α cells, during EPMA data collection, electron beam has more chance to hit the inter-dendritic region than the primary Hcp-(Mg) phase. Thus, the statistical approach used in the work to normalize the measured results linearly within 0 to 1 may not the reasonable and the contribution from the inter-dendritic region could be over-counted.

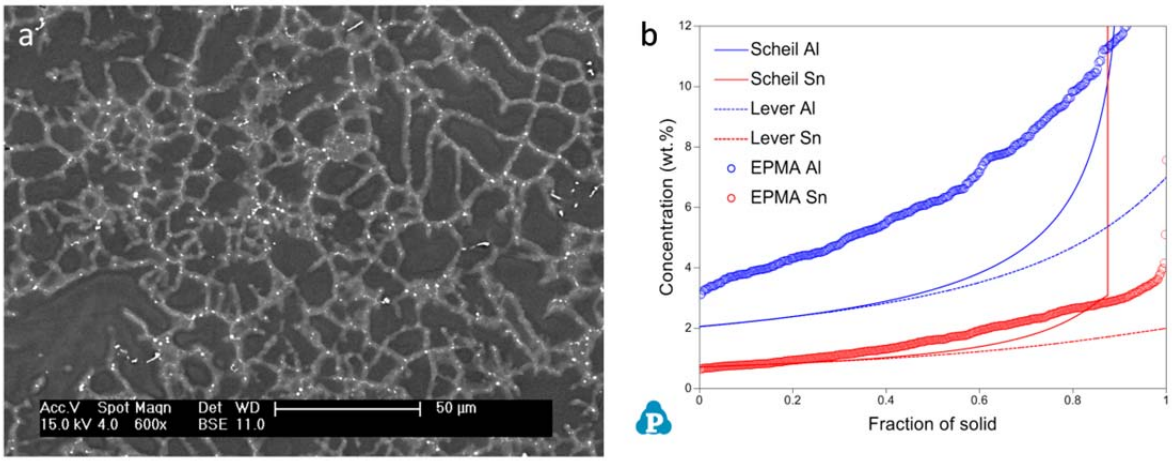

Figure 20. a) the microstructure of die casting AT72 alloy, and b) the calculated concentration profiles of Al and Sn for AT72 alloy using both Scheil and Lever-rule models as compared with experimental results.

The first version of CALPHAD-type Mg atomic mobility database developed within this project for precipitation and solidification simulations includes not only common non-rare earth metals Al, Zn, Sn, Mn, Ca and Sr, but also has been extended to include attractive rare earth metals Ce, Gd, La, Nd and Y, which could significant increase the strength of Mg alloys compared to non-rare earth Mg alloys. During the CALPHAD optimization, the experimental interdiffusion coefficients from this project and literature of Mg-Al, Zn, Y and Gd systems were used to optimize the interaction terms of the atomic mobility parameters. For Sr, the atomic mobility parameter related to impurity diffusion coefficient is directly obtained from first principles calculations [14] since the experiment data are not available. In addition, the interaction term of Al and Zn in Mg is also considered based on the experimental data for ternary MgAlZn systems [25]. This database is being used and tested in heat treatment design, precipitation and solidification simulations. Figures 21 and 22 show that the calculated diffusion coefficients from this atomic mobility database can reproduce most of the experimental results for Mg-Al-Zn [10, 25] and Mg-Gd alloys [25].

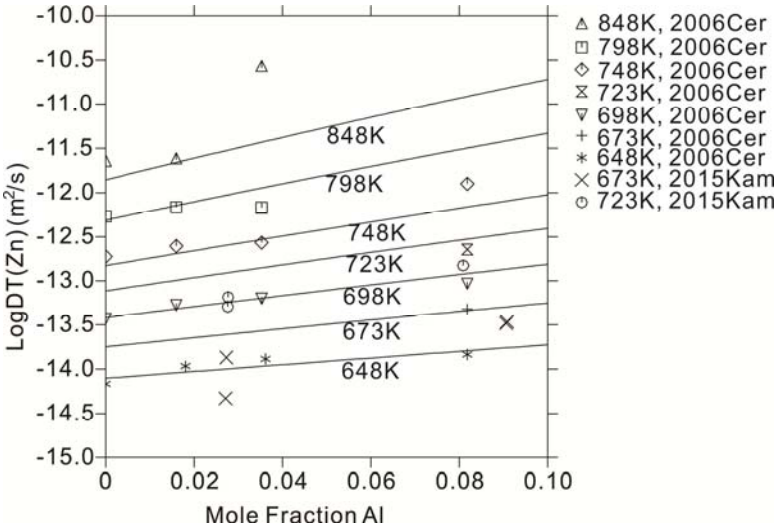

Figure 21. Calculated impurity diffusion coefficients of Zn in Mg-Al alloys with the experimental results [10, 25].

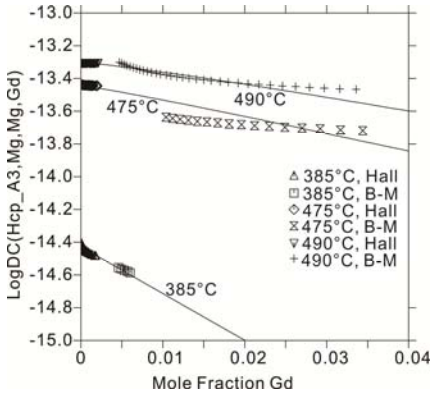

Figure 22. Calculated interdiffusion coefficients in Mg-Gd alloys with the experimental results [25]. The abbreviation B-M represents Boltzmann-Matano method.

Figures 23 and 24 show one case of using the Mg atomic mobility database to assist the design of solution treatment schedule for Mg alloys. The as-cast microstructure of HPDC ATS alloy shown in Fig. 24a exhibits strong segregations of Al and Sn in the grain boundary. Figure 23 shows the simulated composition profiles of Al and Sn in (Mg) during solution treatment at 420°C, which indicates that Al and Sn segregating in the boundary in the as-cast microstructure could be dissolved after 8 hours at 420°C. The as-annealed microstructure presented in Fig. 24b demonstrates that the segregation "cloud" in the as-cast microstructure disappears and the elements Al and Sn segregating in the boundary are dissolved into (Mg) matrix after 8 hours at 420°C.

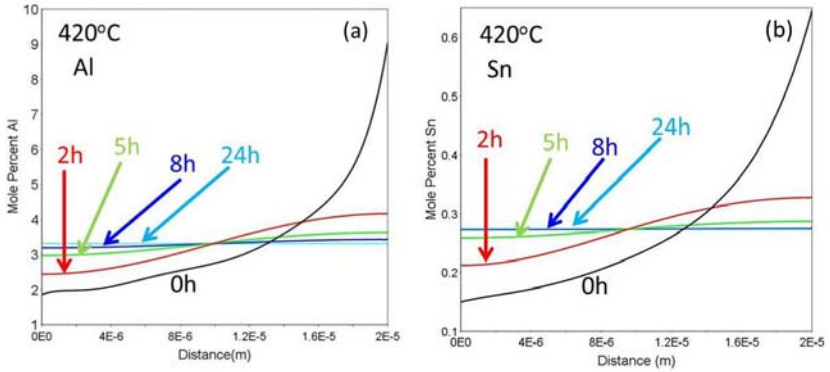

Figure 23. Simulated composition profiles of Al (a) and Sn (b) in (Mg) matrix during solution treatment at 420°C.

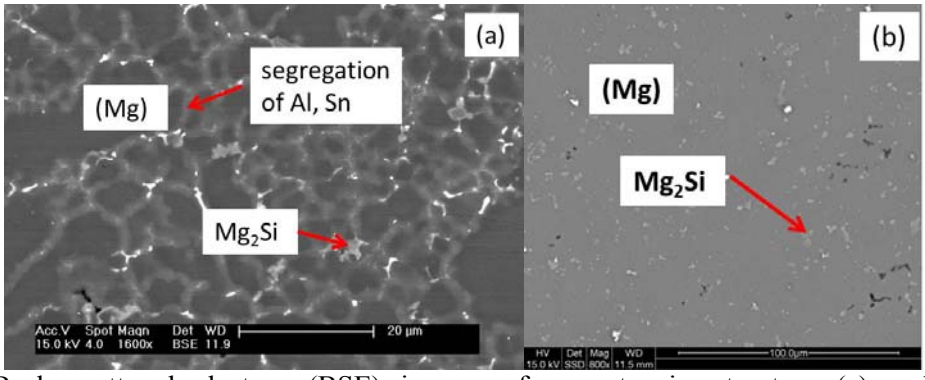

Figure 24. Back scattered electron (BSE) images of as-cast microstructure (a) and as-annealed microstructure at 420°C for 8 hours (b). The Mg_2Si is a highly stable phase and is not dissolved.

The Mg-Al-Ca-Sn alloys were characterized by SEM/EDS and EPMA to get the phase formation and microsegregation. The results were compared with the Scheil-Gulliver simulation. Figure 25 shows themicrostructure of Mg-7.3Al-1.47Ca-0.79Sn and Figure 26 presents the solidification paths from Scheil-Gulliver and equilibrium simulations. The phase formation agrees with Scheil-Gulliver simulation. The primary phase is (Mg), followed by the formation of CaMgSn in the early stage. Ternary compound AlCaMg and $Mg_{17}Al_{12}$ form by eutectic reactions in the later stage. Figure 27 shows the concentration distributions of Al, Ca and Sn in primary (Mg). In Figure 27a, the concentration of Al is higher than that of Scheil-Gulliver simulation. The distribution of Ca is somewhat uniform in Figure 27b. In Figure 17c, the microsegregation of Sn deviates from the simulation. It should be mentioned that in the early stage of the growth of (Mg), another compound CaMgSn will also grow simultaneously, which may influence the redistribution of Ca and Sn.

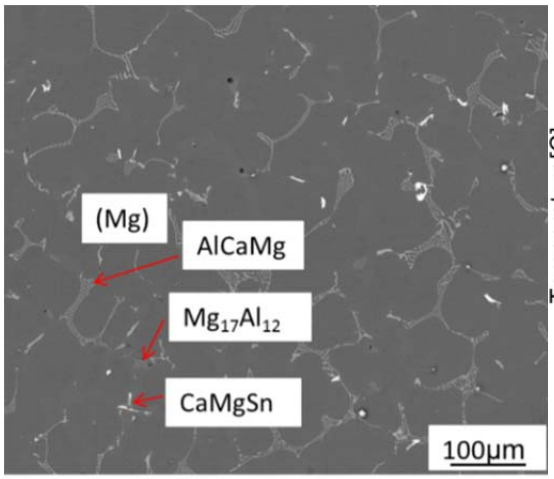

Figure 25. BSE image of Mg-7.3Al-1.47Ca-0.79Sn alloy.

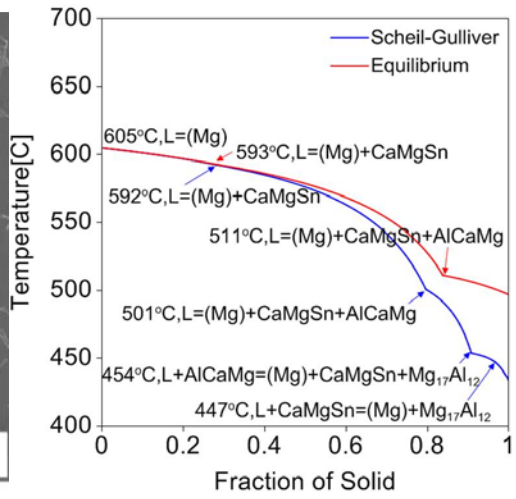

Figure 26. Solidification paths from Scheil-Gulliver and equilibrium simulations for Mg-7.3Al-1.47Ca-0.79Sn alloy.

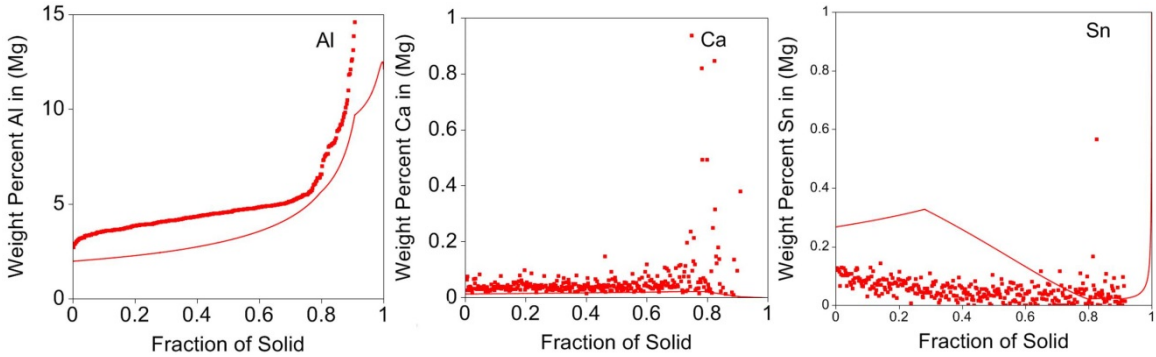

Figure 27. Distributions of the alloying elements in primary (Mg) with the Scheil-Gulliver simulations for Mg-7.3Al-1.47Ca-0.79Sn alloy: (a) Al; (b) Ca; and (c) Sn.

According to the combination of the analysis including X-ray diffraction, SEM/EDS and TEM, the dominant intermetallics in the alloys with high cooling rates (HPDC and steel mold casting) is lamellar $Al_{11}RE_3$and particulate Al_2RE is the minor phase. In the sample prepared by furnace cooling, the amount of Al_2RE phase is increased significantly and comparable with that of $Al_{11}RE_3$, which means high cooling

rate favors the formation of $Al_{11}RE_3$ and decrease the Al_2RE. In addition, high cooling rate refines the microstructure. The eutectic structure consisted of $Mg_{17}Al_{12}$ and (Mg) phase was observed by SEM/EDS in the sample prepared by furnace cooling, as shown in Figure 28a. The site-specific TEM specimen was prepared by focused ion beam and phase crystal structures were confirmed by TEM analysis, as shown in Figure 29. By carefully adjusting the brightness and contrast in the SEM/EDS analysis, the $Mg_{17}Al_{12}$ was also observed in the sample prepared by steel mold casting and confirmed by EDS analysis, as show in Figure 28b.The $Mg_{17}Al_{12}$ phase in the sample prepared by HPDC was not observed, which does not agree with the Scheil-Guiliver simulation as shown in Figure 30.The analysis on the discrepancy indicates that more Al can be trapped in (Mg) during HPDC process.

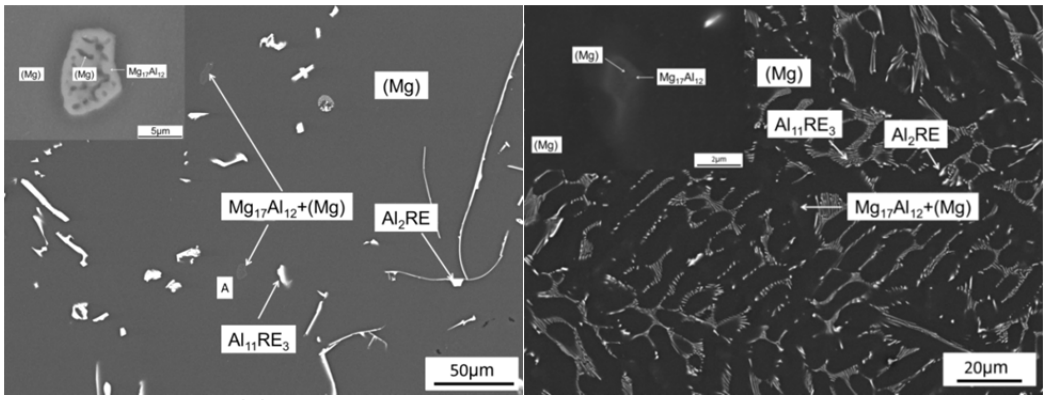

(a) (b)

Figure 28. BSE images of the AE42 samples: (a) Furnace cooling; and (b) steel mold casting.

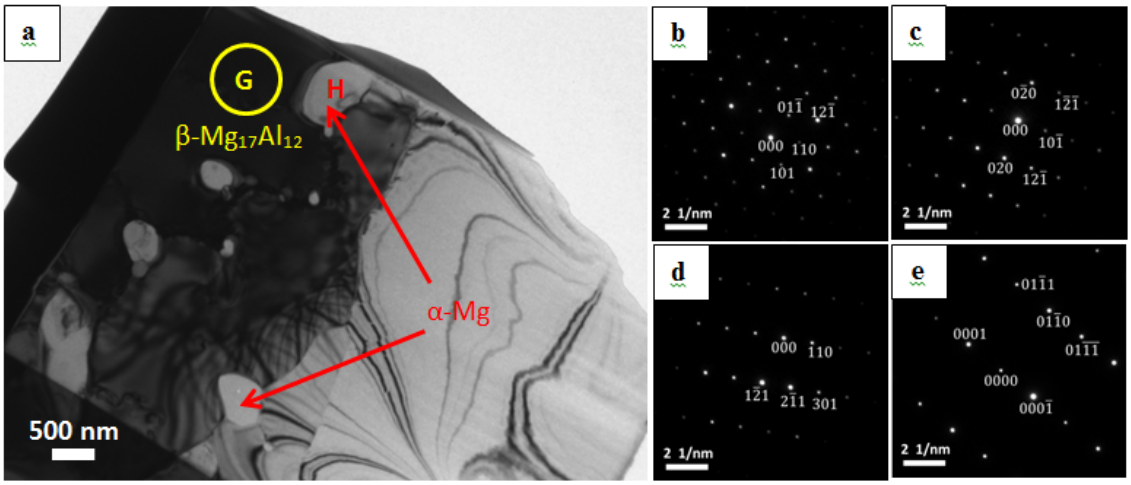

Figure 29. (a) TEM image of $Mg_{17}Al_{12}$; (b)(c)(d) are three different diffraction patterns of area G circled in (a) (B=<1$\bar{1}$1>, <011>, <311>, respectively); and (e) is the diffraction patterns of area H marked in (a).

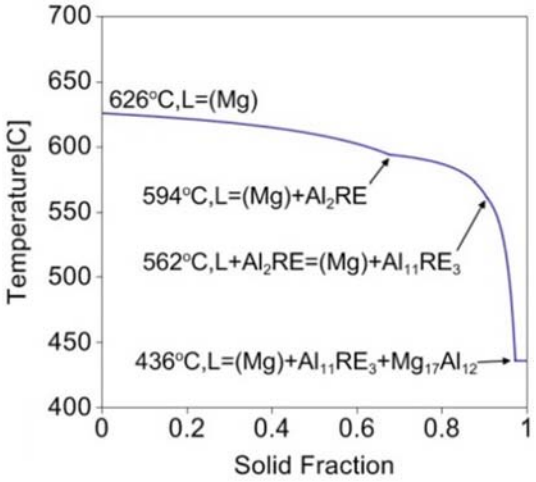

Figure 30. Calculated solidification path of AE42 alloy. The calculation is based on the composition Mg-4Al-2Ce.

Precipitation

Using PanPrecipitation module coupled with PanMagnesium thermodynamic database and the atomic mobility database developed in this project, the precipitation kinetics of Mg_2Sn at 200°C in two supersaturated binary Mg-Sn alloys was simulated. The evolution of precipitation microstructure in Mg-2Sn alloy at 200°C after different aging time is shown in Figure 31. It can be seen that the precipitation process in binary Mg-Sn system is very sluggish. The density of precipitate is still low even after aging at 200°C for 75 hours. Figure 32 shows the simulation of precipitation kinetics in two binary alloys as compared with experimental results. The calculated number density in Figure 32a) for the two Mg-Sn alloys are in agreement with the experimental data. Figure 32b) shows the predicted radius for Mg-1.9 at.%Sn alloy at 240 hours is 128nm, which is consistent with the experimental value of 112nm. However, for the Mg-1.3at.%Sn alloy, the simulated radius at 1000 hours is 160 nm, which is lower than the experimental value of 197 nm, but still close to experimental results. By coupling precipitation kinetics simulation with strength models, the evolution of mechanical property of binary Mg-Sn alloys can be predicted. Different contributions to strengthening also can be revealed. Figure 33 indicates during aging process, the contribution of Mg_2Sn precipitation to yield strength increases while the solution contribution decreases. The predicted hardness evolution is consistent with the experimental data as shown in Figure 34.

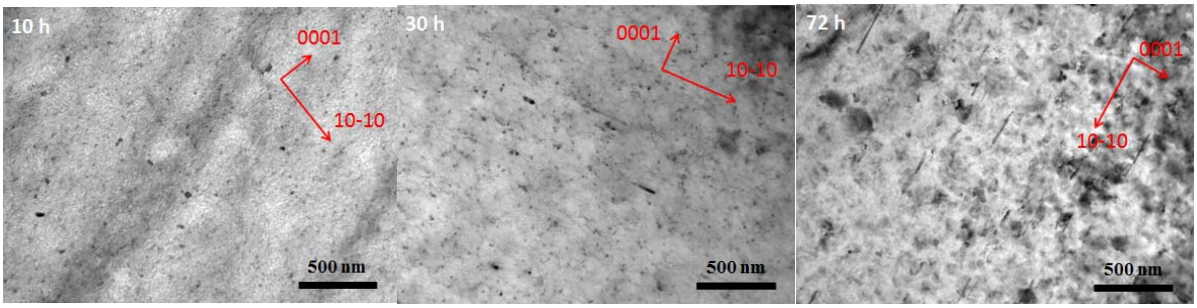

Figure 31. Bright-field TEM images of aged Mg-2Sn alloys at 200ºC for 10, 30 and 72hours with the beam direction close to <11-20>.

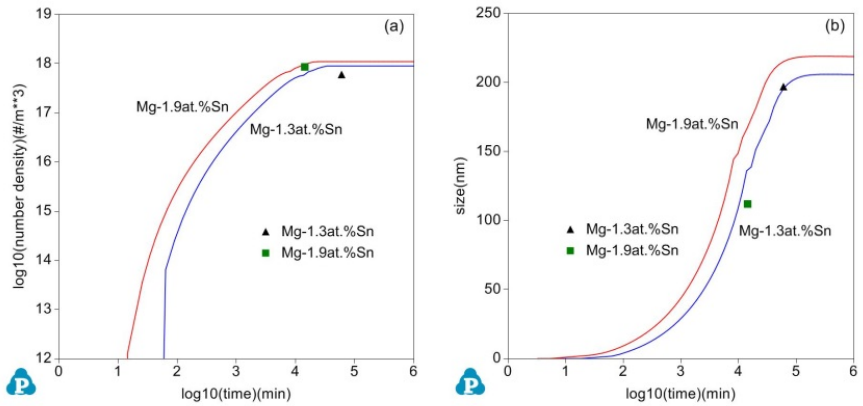

Figure 32. Simulated microstructure of Mg-Sn alloys during aging at 200°C using the new database with experimental data [26]. (a) Number density; and (b) Precipitate size.

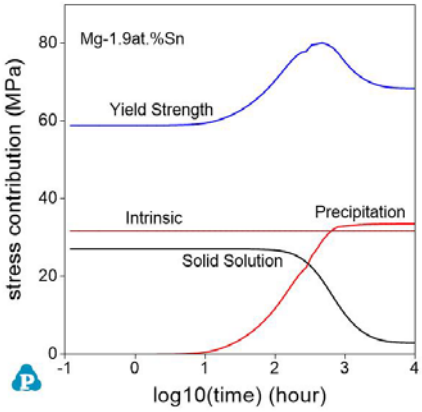

Figure 33. Predicted yield strength including each contribution for Mg-1.9 at.%Sn.

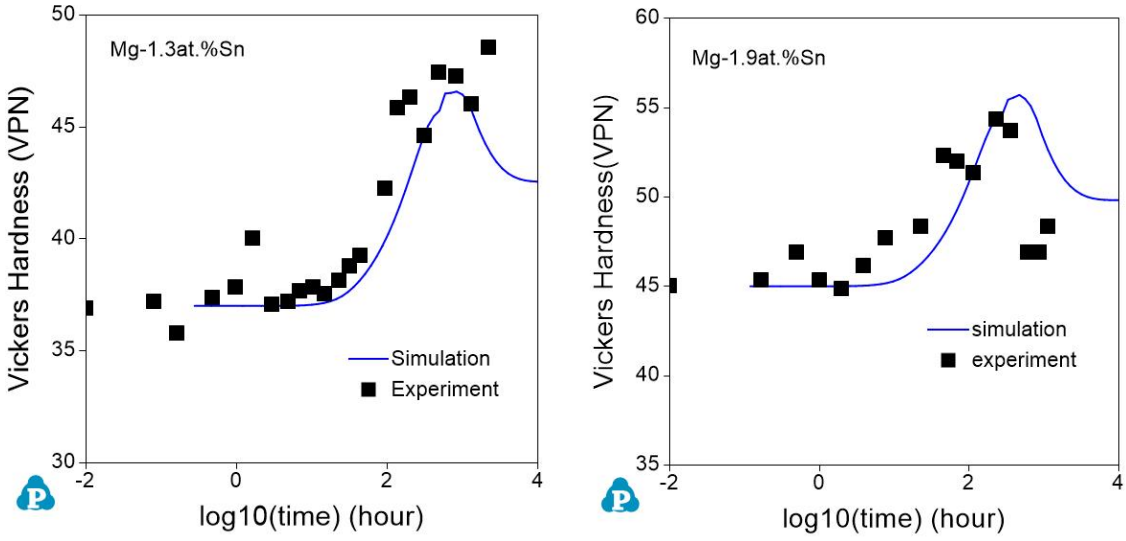

Fig. 34. Predicted hardness evolution with the experimental data [26]. (a) Mg-1.3 at.%Sn; and (b) Mg-1.9at.%Sn.

The evolution of precipitates $Mg_{17}Al_{12}$ in another important commercial magnesium alloy AZ91 was also simulated using PanPrecipitation module coupling with the newly developed mobility database. The simulated number density, average radius and volume fraction of $Mg_{17}Al_{12}$ at 200°C with the experimental data are shown in Fig. 35. It can be seen that the simulation results are consistent with experimental results.

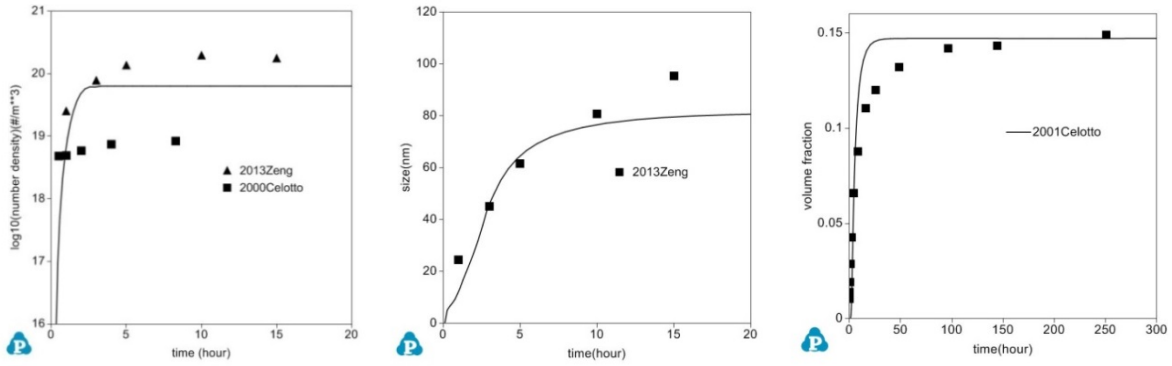

(a) (b) (c)

Fig. 35. Predicted (a) number density, (b) size, (c) volume fraction of $Mg_{17}Al_{12}$ precipitate in Mg-9Al-1Zn alloy at 200°C with the experimental data [27-29].

By combining the parameters for Mg_2Sn and $Mg_{17}Al_{12}$, the concurrent simulation of precipitation of $Mg_{17}Al_{12}$ and Mg_2Sn in Mg-7Al-2Sn (wt.%) alloys is simulated. Figure 36 shows the bright field TEM images of Mg-7Al-2Sn alloys at 200ºC for 10, 30and 72hours. The number of precipitates is growing as time increases and coarsening already happens at 72hours. Figure 37 a) shows the high-angle annular dark field-scanning transmission electron microscope (HAADF-STEM) image of the AT72 sample aged for 72 hours. STEM-EDS was used to distinguish Mg_2Sn and $Mg_{17}Al_{12}$precipitates as shown in Figure 37 b)-d). The foil thickness for calculating the number density is measured using Zero-loss Electron Energy Loss (EELS) Spectrum. Figure 37 e) shows an example of Zero-loss EELS spectrum obtained from A AT72 TEM specimen. Fig. 38 shows the predicted microstructure evolution of Mg_2Sn and $Mg_{17}Al_{12}$. From simulation, it is concluded that the precipitation of $Mg_{17}Al_{12}$ is much stronger than that of Mg_2Sn. the precipitation of Mg_2Sn in binary alloy is very sluggish. By comparison with simulation results presented in Figure 32, it can be seen that the precipitation of Mg_2Sn in the ternary alloy was greatly accelerated.

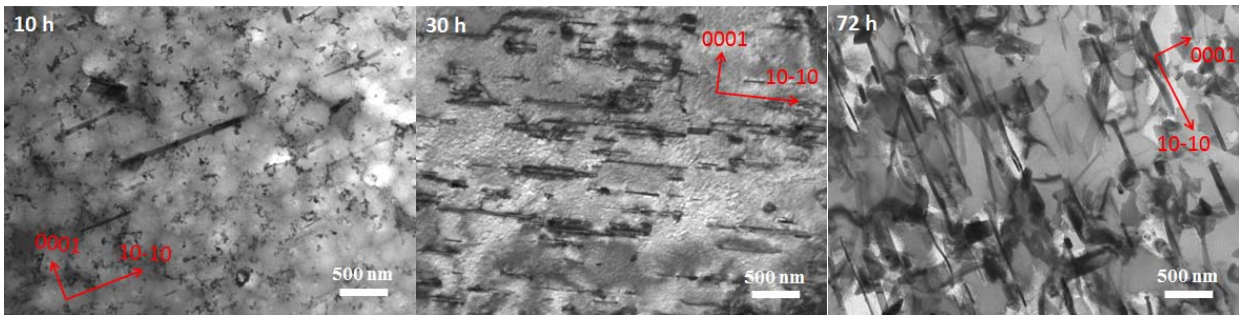

Figure 36. Bright field TEM images of aged Mg-7Al-2Sn alloys at 200ºC for 10, 30, and 72hours with the beam direction close to <11-20>.

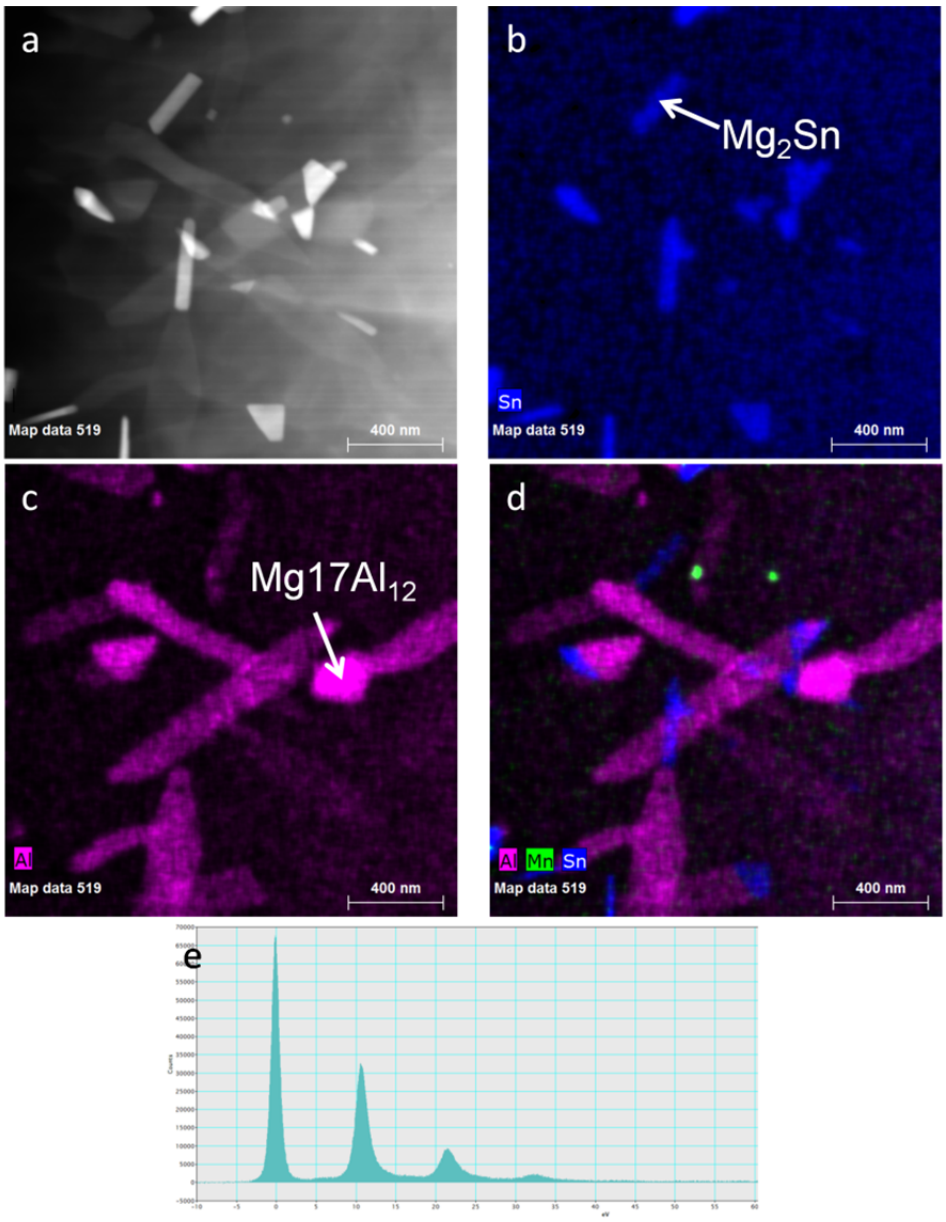

Figure 37. STEM/STEM-EDS characterization of AT72 microstructure aged at 200°C for 72 hours: a) HAADF-STEM image; b) Sn EDS map; b) Al EDS map; c) overlapped elements map; and e) zero-loss EELS spectrum.

In order to study the alloying effects on precipitation kinetics in AT72 alloy, the alloy were further microalloyed with Zn, Ag, Cu and Ca. All test specimens were prepared using gravity casting in steel molds. The aging hardening responses of different microalloyed AT72 specimens at 200°C are shown in Fig. 39. It can be that small amount of addition of Zn (0.6 wt.%) or Ag (0.7 wt.%) can greatly accelerate the aging hardening of AT72 alloys. Large amount of Ag (4 wt.%) further increases the hardness, but not significantly. Cu enhances the hardness, but doesn't accelerate the aging response. Ca has negative effect on the aging hardening of AT72 alloy. Thus, micro alloying may be an effective method further optimizes the mechanical properties of Mg-Sn systems.

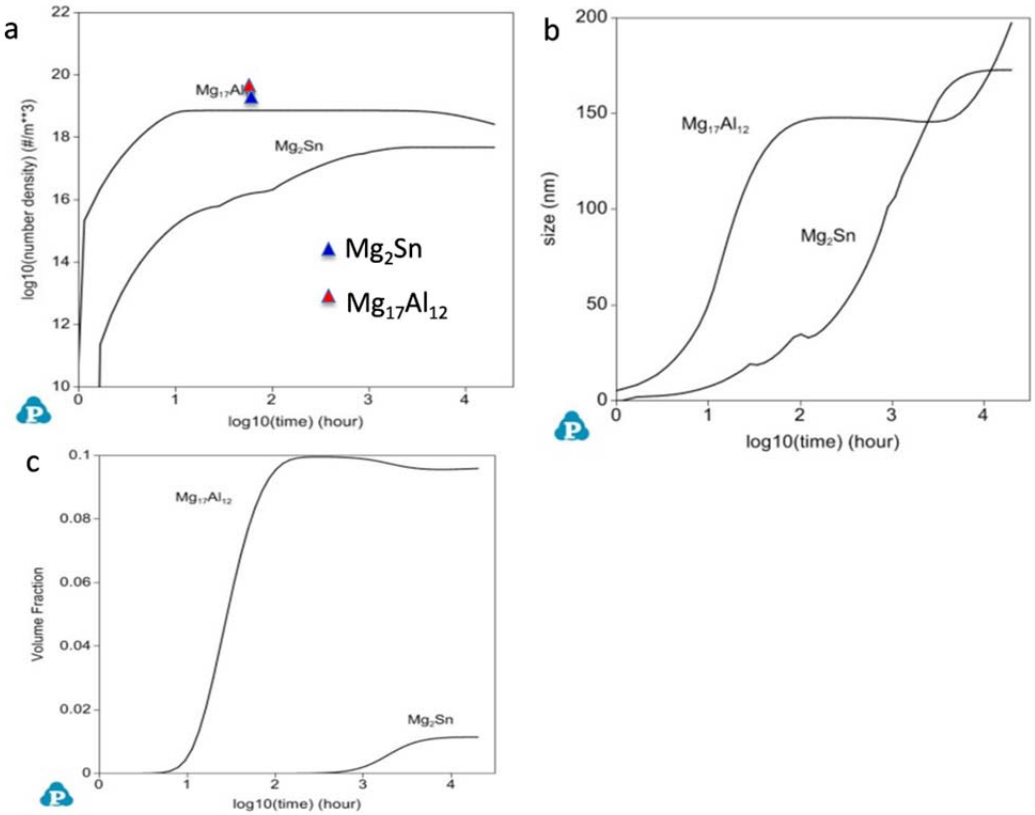

Figure 38. Precipitation kinetics simulated using PanPrecipitation module coupling the newly developed mobility database: (a) number density; (b) size; and (c) volume fraction of $Mg_{17}Al_{12}$ and Mg_2Sn precipitates in Mg-7Al-2Sn alloy at 200°C.

Technology Transfer Path

The project has produced the following technological accomplishments:

- The diffusivities measured in this work significantly improve the mobility database for Mg alloys, which is rather inadequate, compared with that of Al alloys. These experimental data lay the foundation for investigation of diffusion of alloying elements in Mg and can assist the design of high performance Mg alloys using an Integrated Computational Materials Engineering approach.
- Through coupling to Mg thermodynamic database, the established CALPHAD-type Mg atomic mobility database can conveniently calculate or extrapolate composition and temperature dependent diffusion coefficients for precipitation and solidification simulations in process design for Mg alloys.
- The PanSolidification module can be used to predict more accurate microstructure evolution of Mg alloys during casting process such as solidification path, microsegregation and second arm spacing once fully developed.
- The research on the precipitation and microalloying of AT72 alloy indicates (1) Precipitation of Mg_2Sn can be enhanced and accelerated via microalloying; (2) Zn and Ag may further improve the aging hardening response of AT72 alloy.

The project team is working closely with the automotive industry (collaborating with General Motors) to promote Mg castings for lightweight applications. The following are some example:

- The new mobility database and solidification and precipitation models are being used to optimize Mg-Al-Sn based cast alloys for high-strength applications.
- AT72 alloy was successfully used to cast a lightweight Mg door inner (Figure 40), which was 2.7 kilogram and achieved about 50% mass saving compared with the baseline steel door design. GM is presently testing the door inner for potential applications in the future.

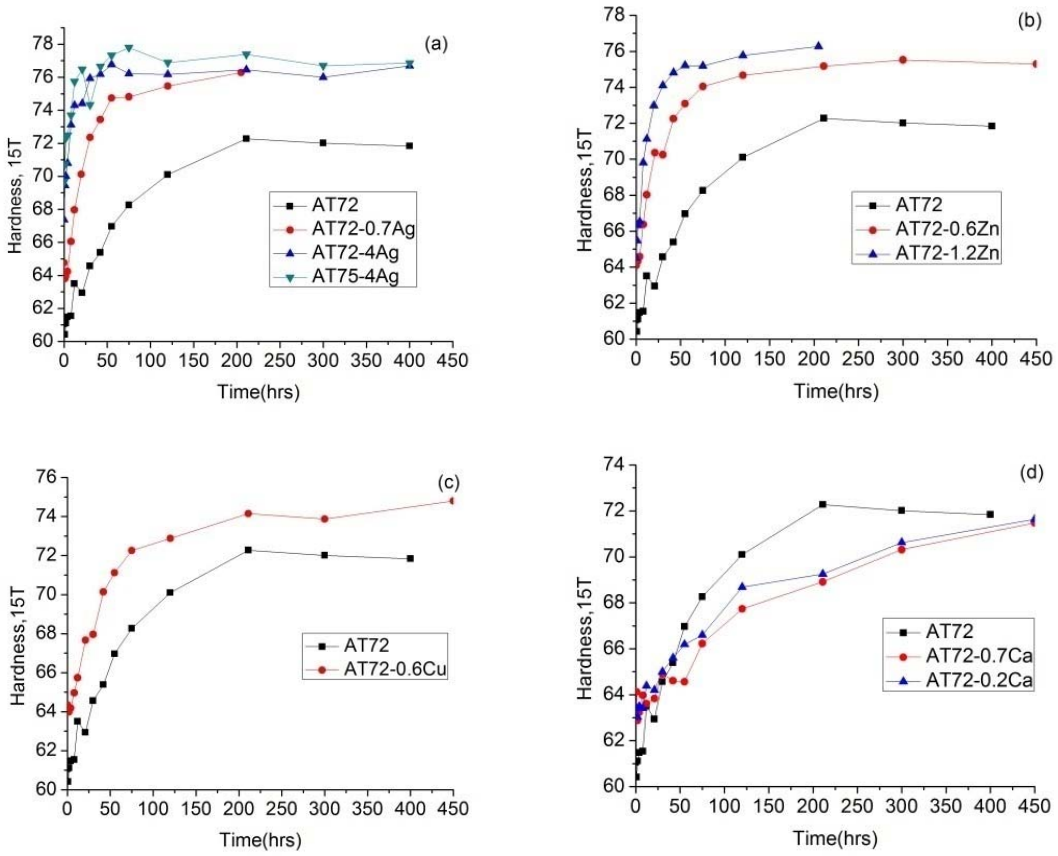

Figure 39. Aging hardening responses of AT72 alloys microalloyed with Ag, Zn, Cu and Ca. (a) Ag; (b) Zn; (c) Cu; and (4) Ca.

Figure 40. AT72 Mg door inner die casting (in collaboration with General Motors).

Conclusions

1. Reliable diffusivities for Mg-Al, Zn, Sn, Ca and Y systems were obtained by a combination of high throughput diffusion multiple/liquid-solid diffusion couple experiments and the forward simulation. Liquid-solid diffusion couples including Mg-MgNd, MgY, MgGd, MgCe, MgMn, Li and Sr systems were prepared and some diffusion profiles were obtained.

2. CALPHAD-type Mg atomic mobility database including 11 elements within this project was collected based on assessment and optimization of the experimental data within this project and literature. This new database was used in the design of solution treatment schedule, precipitation and solidification simulations of Mg alloys.

3. Phase transformation kinetics during casting processes of various Mg alloys for automotive applications were studied in this work using both experimental methods coupled with simulations. A CALPHAD-based solidification micromodel, PanSolidification taking into account of both back diffusion in the solid phase and the geometrical dendrite structure, was successfully used for modeling solidification microstructures in Mg alloys. This micromodel can be used to simulate the microsegregation and dendrite structure in different solidification conditions from slow cooling in directional solidification to fast cooling in high pressure die casting. The simulation results show good agreement with experimental measurements.

4. The evolution of precipitation microstructure in Mg-Al-Sn based alloys was investigated in this work. A KWN-based model, PanPrecipitation coupling the PanMg thermodynamic database and the mobility database developed in this work, was used to simulate the precipitation kinetics and mechanical properties. The simulation results on binary Mg-Sn and Mg-Al were comparable to the experimental results. Further study is being carried out to extend the current precipitation model to Mg-Al-Sn ternary systems with co-precipitation microstructure.

5. Alloying additions have significant effects on precipitation kinetics of Mg alloys. Ag and Zn addition can greatly enhance and accelerate the precipitation kinetics in Mg-Sn system, while other alloying elements such as Ca and Cu have detrimental effects.

Acknowledgment:

This material is based upon work supported by the Department of Energy Award Number DE-EE0006450.

Disclaimer:

References

[1] Zhang, Q.; Zhao, J.C. "Extracting Interdiffusion Coefficients from Binary Diffusion Couples Using Traditional Methods and a Forward-Simulation Method." *Intermetallics* (34), 2013; pp. 132-141.
[2] Saunders, N.; Miodownik, A.P., ed. *CALPHAD (Calculation of Phase Diagrams): A Comprehensive Guide*, Oxford: Pergemon Press, 1998.
[3] Kampmann, R.; Wagner, R. "Kinetics of Precipitation in Metastable Binary Alloys-theory and application to Cu-1.9 at % Ti and Ni-14 at % Al." *Decomposition of Alloys: the Early Stages*. September 19-23, 1983, Sonnenberg, Germany. Oxford: Pergamon Press, 1983; pp. 91-103.
[4] Zhang, C.; Cao, W.; Chen, S.L.; Zhu, J.; Zhang, F.; Luo, A.A.; Schmid-Fetzer, R. "Precipitation Simulation of AZ91 Alloy." *JOM* (66:3), 2014; pp. 389-396.
[5] Kammerer, C.C.; Kulkarni, N.S.; Warmack, R.J.; Sohn, Y.H. "Interdiffusion and Impurity Diffusion in Polycrystalline Mg Solid Solution with Al or Zn." *Journal of Alloys and Compounds* (617), 2014; pp. 968-974.
[6] Brennan, S.; Bermudez, K.; Kulkarni, N.S.; Sohn, Y.H. "Interdiffusion in the MG-Al System and Intrinsic Diffusion in β-Mg2Al3." *Metallurgical and Materials Transactions A* (43:11), 2012; pp. 4043-4052.
[7] Das, S.K.; Kim, Y.M.; Ha, T.K.; Gauvin, R.; Jung, I.H. "Anisotropic Diffusion Behavior of Al in Mg: Diffusion Couple Study Using Mg Single Crystal." *Metallurgical and Materials Transactions A* (44: 6), 2013; pp. 2539-2547.
[8] Brennan, S.; Warren, A.P.; Coffey, K.R.; Kulkarni, N.; Todd, P.; Kilmov, M.; Sohn, Y.H. "Aluminum Impurity Diffusion in Magnesium." *Journal of phase Equilibria and Diffusion* (33:2), 2012; pp. 121-125.
[9] Lal, Krishan. *L'Étude de la diffusion de quelques éléments dans le magnésium*. Ph.D. Dissertation. Paris, France: University of Paris, 1967.
[10] Čermák, J.; Stloukal, I. "Diffusion of 65Zn in Mg and in Mg–x Al Solid Solutions." *Physica Status Solidi (a)* (203:10), 2006; pp. 2386-2392.
[11] Das, S.K.; Kim, Y.M.; Ha, T.K.; Jung, I.H. "Investigation of Anisotropic Diffusion Behavior of Zn in HCP Mg and Interdiffusion Coefficients of Intermediate Phases in the Mg–Zn System." *Calphad* (42), 2013; pp. 51-58.
[12] Combronde, J.; Brebec, G. "Heterodiffusion de Ag, Cd, In, Sn et Sb dans le magnesium." *Acta Metallurgica* (20:1), 1972; pp. 37-44.
[13] Das, S.K.; Kang, Y.B.; Ha, T.K.; Jung, I.H. "Thermodynamic Modeling and Diffusion Kinetic Experiments of Binary Mg–Gd and Mg–Y Systems." *Acta Materialia* (71), 2014; pp. 164-175.
[14] Zhou, B.C.; Shang, S.L.; Wang, Y.; Liu, Z.K. "Diffusion Coefficients of Alloying Elements in Dilute Mg Alloys: A Comprehensive First-principles Study." *Acta Materialia* (103), 2016; pp. 573-586.
[15] Ganeshan, S.; Hector, L.G.; Liu, Z.K. "First-Principles Calculations of Impurity Diffusion Coefficients in Dilute Mg Alloys Using the 8-Frequency Model." *Acta Materialia* (59:8), 2011; pp. 3214-3228.
[16] Wu, Henry, Tam Mayeshiba, and Dane Morgan. "High-Throughput ab-initio Dilute Solute Diffusion Database." *arXiv preprint arXiv:1602.01725* (2016).
[17] Nandipati, G.; Govind, N.; Andersen, A.; Rohatgi, A. "Self-Learning Kinetic Monte Carlo Simulations of Al Diffusion in Mg." *Journal of Physics: Condensed Matter* (28:15), 2016; 155001.
[18] Combronde, J.; Brebec, G. "Anisotropie d'autodiffusion du magnesium." *Acta Metallurgica* (19:12), 1971; 1393-1399.
[19] M,N.Gungor, A statistically significant experimental technique for investigating microsegrgation in cast alloys, Metallurgical Transactions A, Vol.20A, (1989), p2529-2533.
[20] Zhang, C.; Ma, D.; Wu, K.S.; Cao, H.B.; Cao, G.P.; Kou, S.; Chang, Y.A.; Yan, X.Y. "Microstructure and microsegregation in directionally solidified Mg-4Al alloy." *Intermetallics* (15:10), 2007; pp. 1395-1400
[21]Paliwal, M.; Jung, I.H. "The Evolution of the Growth Morphology in Mg–Al Alloys Depending on the Cooling Rate during Solidification." *ActaMetallurgica*(61:13), 2013; pp. 4848-4860.
[22]Paliwal, M. *Microstructural Development in Mg Alloys during Solidification: An Experimental and Modeling Study*. Ph.D. Thesis. Montreal, QC: McGill University, 2013.
[23] Zheng, X.W.; Luo, A.A.; Zhang, C.; Dong, J.; Waldo, R.A. "Directional Solidification and Microsegregation in a Magnesium-Aluminum-Calcium Alloy."*Metallurgical and Materials Transactions A* (43:9), 2012; pp. 3239-3248.

[24]Paliwal, M.; Jung, I.H. "Solid/Liquid Interfacial Energy of Mg-Al Alloys." *Metallurgical and Materials Transactions A* (44:4), 2013; pp. 1636-1640.
[25] Kammerer, C.C. *The Influence of Alloying Additions on Diffusion and Strengthening of Magnesium*. Ph.D. Thesis. Orlando, FL: University of Central Florida, 2015.
[26] Mendis, C. L.; Bettles, C. J.; Gibson, M. A.; Gorsse, S.; Hutchinson, C. R. "Refinement of Precipitate Distributions in an Age-Hardenable Mg–Sn Alloy through Microalloying." *Philosophical Magazine Letters* (86:7), 2006; pp. 443-456.
[27]Zeng R. *Precipitation Hardening in AZ91 Magnesium Alloy*. Ph.D. Thesis. Birmingham, UK: University of Birmingham, 2013.
[28]Celotto, S. "TEM Study of Continuous Precipitation in Mg–9 wt% Al–1 wt% Zn Alloy." *ActaMetallurgica* (48:8), 2000; pp. 1775-1787.
[29]Celotto, S.; Bastow, T. J. "Study of Precipitation in Aged Binary Mg–Al and Ternary Mg–Al–Zn Alloys Using ^{27}Al NMR Spectroscopy." *ActaMetallurgica* (49:1), 2001; pp. 41-51.

BIBLIOGRAPHY (PRESENTATIONS/PUBLICATIONS/PATENTS)

Publications:

1. Luo, A.A.; Sun, W.; Zhong, W.; Zhao, J.C., "Computational Thermodynamics and Kinetics for Magnesium Alloy Development", Advanced Materials and Processes, 2015, 173, (1), 26-30.
2. Sun, W.H.; Zhang C.; Klarner A.D.; Cao W.; Luo A.A., "Simulation of concurrent precipitation of two strengthening phases in magnesium alloys", Magnesium Technology 2015, Edited by: Michele V. Manuel et al., TMS, 2015, 289-293.
3. W. Zhong, J.C. Zhao, "First experimental measurement of calcium diffusion in magnesium using novel liquid-solid diffusion couples and forward-simulation analysis", Scr. Mater. 2017(127), pp 92-96.
4. W.H. Sun, X.Y. Shi, E. Cinkilic, A.A. Luo, "Investigation of the non-equilibrium solidification microstructure of a Mg-4Al-2RE (AE42) alloy", J. Mater. Sci., 2016(51), pp 6287-6294.
5. S. Shang, Z. Han, W. Sun, A.A. Luo, "A Phase Field Model Coupled with Pressure-effect-embedded Thermodynamic Modeling for Describing Microstructure and Microsegregation in Pressurized Solidification of A Ternary Magnesium Alloy", Computational Materials Science, 2017, 136, 264–270.
6. A.A. Luo, "Material Design and Development: from Classical Thermodynamics to CALPHAD and ICME Approaches", CALPHAD: Computer Coupling of Phase Diagrams and Thermochemistry, 2015, 50, 6-22.

Presentations:

1. A.A. Luo, "Magnesium Alloy Design and Process Development Using Integrated Computational Materials Engineering (ICME) Approaches," Invited Talk, Magnesium Workshop, Johns Hopkins University, Baltimore, MD, April 3 - 4, 2017.
2. A.A. Luo, "Integrated Computational Materials Engineering for Automotive Light Metals", Invited Talk, TMS Annual Meeting, San Diego, CA, USA, February 27-March 2, 2017.
3. A.A. Luo, W. Sun, E. Cinkilic, Z. Liang, "Application of CALPHAD Modeling in the Development of Light Metals," CALPHAD XLV Conference, Awaji, Japan, May 29 - June 3, 2016.
4. A.A. Luo, "Advanced Light Metals and Manufacturing for Structural Applications," Keynote Talk, Materials Science and Technology 2016, Salt Lake City, UT, October 23-27, 2016.
5. A.A. Luo, "The Role of Integrated Computational Materials Engineering (ICME) in Light Alloy Development and Advanced Processing," Invited Talk, Arkema Materials Science and Engineering Seminar, Pennsylvania State University, University Park, PA, October 20, 2016.
6. Zhong, W., Sun, W., Zhao, J.C., Luo, A.A., "Establish a Mg Diffusivity Database using Diffusion Multiples and Liquid-Solid Diffusion Couples", MS&T2015, October 4-8, 2015, Columbus, OH

7. Sun, W., Zhang C., Zhong, W., Luo, A.A., Zhao, J.C., "Investigation of Microstructure and Microsegregation during Solidification of Mg Alloys", MS&T2015, October 4-8, 2015, Columbus, OH
8. Zhong, W.; Sun, W.; Zhao, J.C.; Luo, A.A., "Establishment of Mg Diffusivity Database Using Diffusion-Multiple and CALPHAD Approaches", Computational Thermodynamics and Kinetics, TMS 2015 144th Annual Meeting & Exhibition, March 15-19, 2015, Orlando, FL.
9. Sun, W.; Zhang, C.; Klarner, A.D.; Cao, W.; Luo, A.A., "Simulation of Concurrent Precipitation of Two Strengthening Phases in Magnesium Alloys", Magnesium Technology 2015, TMS 2015 144th Annual Meeting & Exhibition, March 15-19, 2015, Orlando, FL.